INTERNATIONAL BUILDING PERFORMANCE SIMULATION ASSOCIATION ENGLAND

Proceedings of BSO-V 2020
5th Building Simulation and Optimization Virtual Conference
21-22 September 2020
Loughborough, UK

Estimation of Global Thermal Performances of a Facade Under Real Climate

Manon Rendu[1,2], Jérôme Le Dréau[1,2], Maxime Doya[3], Patrick Salagnac[1,2]
[1] LaSIE, La Rochelle University, CNRS, UMR 7356, La Rochelle, France
[2] 4evLab, La Rochelle University, CNRS, Electricité de France EDF, La Rochelle, France
[3] TIPEE Platform, Lagord, France

Abstract

The article aims at estimating the thermal characteristics of a facade component (highly insulated wall with a window) installed on a test cell using an inverse method. The test cell is used as a calorimeter to estimate the global properties of the facade component (including thermal bridges). The characteristics of interest are the thermal resistances and capacities and the effective window area but the thermal properties of the test cell also need to be identified as the heat balance is performed at the cell level. The problem commonly met is the correlation of a large number of parameters to be estimated and it is therefore difficult to assess physical parameters.

The methodology consists in performing two experimental tests with different temperature scenarios using a heating system and thus allowing the interior and exterior conditions to be decoupled during identification. Then, the two experimental tests were assigned to two different Resistance-Capacitance models, depending on the quality of the data. The higher the quality of the test, the more complex the model is. The purpose is to take advantage of the differences between the two experimental tests to carry out identification by parts, i.e. to estimate the parameters one after the other using the most appropriate Resistance-Capacitance model.

All estimated parameters are close to the theoretical values. The gap is greater for the effective window area, which might come from the assumption of a constant value over the evaluated period. This parameter depends on direct solar radiation. An additional specific test could resolve this challenge. Moreover, the thermal resistance of the facade is underestimated. Thermal bridges may have been missed in the calculation of the target value.

Nomenclature

A	area, m²
C	thermal capacity, kWh.K^{-1}
L	likelihood function
P	power, W
R	thermal resistance, K.W^{-1}
T	temperature, °C

Indices and exponents

c	test cell	i	indoor
e	enters the opaque wall	o	outdoor
f	facade	sol	solar
f/w	facade except window	TG	thermal guard
h	heating	w	window

Introduction

Estimating the thermal performances of facades is a real challenge today since these buildings' components are more and more complex (Freitas and Brito 2019; Agathokleous and Kalogirou 2016). For example, they integrate dynamic heat storage or dynamic control of solar gains by adjusting the solar factor of glazing. (Favoino et al. 2018) explains that, in the case of adaptive facades, "the intrinsic complexity of the dynamic behaviour […] when compared to traditional building envelope components, leads to the fact that conventional simulation tools, experimental assessment methods […] cannot be fully adopted in the case of adaptive facades.".

This implies modelling issues (Attia et al. 2018) (significant complex physical phenomena, cumbersome modelling). As shown in (Roels et al. 2017), it is necessary to define reliable and robust methodologies because existing methodologies can lead to very different results.

Moreover, experimental facilities evolve. In addition to laboratory experiments on samples, occupied buildings or test cells are often used to evaluate the thermal performance of such buildings' components under real climatic conditions (Cattarin et al. 2016). Indeed, the performances of new facade components are highly influenced by the outdoor climate.

In this article, the facade is built on a test cell. The purpose is to determine the "global" thermal characteristics of a highly insulated facade with a double-glazed window, namely, the thermal resistances and capacities and the effective window area. It is necessary to assess these characteristics and make sure that they are not correlated with the characteristics of the thermal guard.

None of the available methods seem to address this issue. Many articles deal with opaque walls and only estimate their thermal resistance (Yang 2017; Gaspar, Casals, and Gangolells 2018; Pflug et al. 2018; Ficco et al. 2015; Naveros et al. 2014). Some of them also estimate capacities (Gori et al. 2017). Other articles deal with building models and solar gains (Jiménez, Porcar, and Heras 2008; Roels et al. 2017) but do not take into account several boundary conditions as is the case in a guarded test cell. When several boundary conditions are taken into account, overall losses are often evaluated (Juricic et al. 2019). Whatever the example, the physical interpretation of the identified parameters is an issue (Raillon and Ghiaus 2018; Juricic et al. 2018). The development of a

new methodology to estimate the different parameters of the test cell is thus useful.
First, the methodology is briefly introduced. Next, the experimental facility and data are described. Then, the modelling aspects are explained and the calculation of the target values of the parameters is outlined. Finally, the results are presented.

Overview of the Methodology

The estimation of model parameters is a feasible task, but the estimated parameters are highly correlated and therefore the estimated values are generally not realistic. The covariance matrices highlight it. Instead of a global identification, it is thus decided to perform identification by parts, i.e. the parameters are estimated separately. To do so, a large amount of data is required. Therefore, two experimental tests with different temperature scenarios are performed. A RC model is related to each dataset since some disparities exist between both datasets, mainly with respect to the frequencies involved. The simplest model enables the estimation of global parameters such as the total resistance of walls and the most detailed model helps to determine more specific parameters such as the resistance of the window.

Experimental Facility and Data

The experimental facility is made up of a test cell (*c*), a thermal guard (*TG*) and a facade (*f*).

General Outline

The experimental facility is a building equipped with testing envelopes located in La Rochelle, France. The building acts as a thermal guard room surrounding the test cells. The test cells are rooms with five highly insulated walls surrounded by the thermal guard mentioned above, in order to maximize the heat flow through its sixth wall, called *facade* facing the outdoor climate.

The Test Cell

A layout of the facility is given in Figure 1.

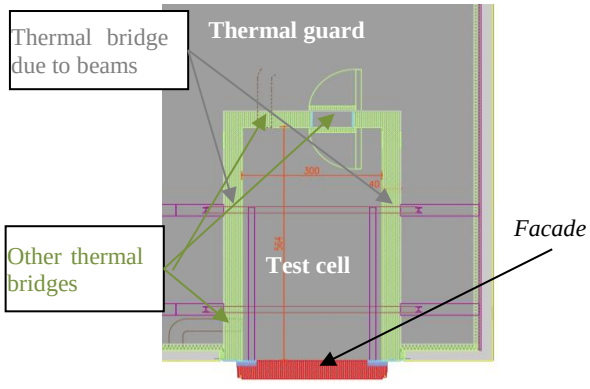

Figure 1: Layout of the facility – top view

The test cell that hosts the *facade* of interest is 5.64 meters long, 3 meters wide and 3 meters high (internal dimensions). Its internal walls are built with 40 cm thick polyurethane foam panels. The *facade* is supported by four composite beams to ensure its contact with the building. The steel connectors are shown in the red rectangle of Figure 2-b.

Composite beams cross the walls of the cell eight times. It causes a thermal bridge called *thermal bridge due to the beams*. Other thermal bridges are due to the ventilation and the hydraulic systems, the cable duct and the door. These thermal bridges are called *other thermal bridges*.
A 1500 W electric heater provides heating in the cell. A fan homogenizes the air temperature in the room.

The *Facade* Component Under Test

The *facade* is shown from outside and inside in Figure 2. The four corners (in green in Figure 2 (c)) consist of a wooden frame to fasten the *facade* to the building. This frame is surrounded by extruded polystyrene (*XPS*) to reduce heat losses. A white metal cover positioned all around the *facade* provides a watertight seal and also strengthens the insulation along the four corners. A window consisting of a PVC frame and a double glazing is located in the middle of the *facade*. The 4 mm thick panes are separated from each other by 16 mm and the cavity is filled with argon gas. A low emissivity coating is placed on the inner pane. Another wooden frame filled with 220 mm-thick *XPS* is located between the window and the first wooden frame. The assembly is closed with two 21 mm-thick Bakelite-coated plywood panels (*Pl*).

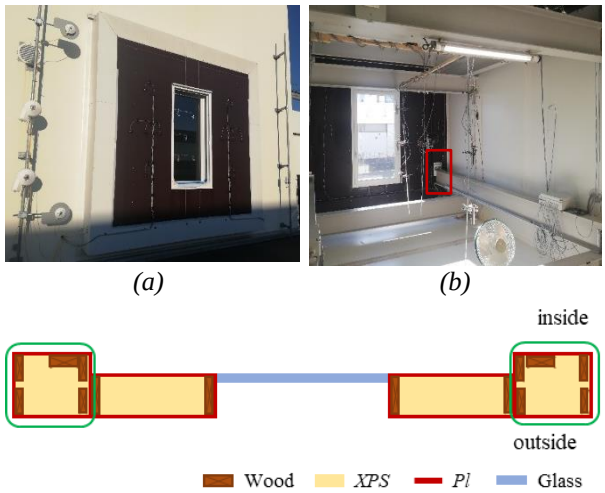

(a) *(b)*

(c)

Figure 2: Outside (a) and inside (b) of the test cell (c) Layout of the facade – top view

Measurements

The air temperatures in the test cell and in the thermal guard are measured by shielded Pt100 temperature sensors. Six sensors are in the test cell and four sensors are in the thermal guard. A fully equipped weather station measures the outdoor weather conditions located on the roof of the building: air temperature, short wave and long wave solar radiations. These physical quantities are also measured near the *facade*. The uncertainty of temperature measurements is estimated to be ± 0.15°C. The uncertainty of the shortwave radiation measurements is ± 3 W/m².
The electrical power demand of the electric heater is measured by a high precision power meter (Sineax DM5). Its accuracy is ±1%. The sampling time step is one minute.

Experimental Datasets

Two experimental datasets were used. The data are shown in Figure 3 and Figure 4. The first one lasted 12 days: 6 days of constant power (200 W) heating step and 6 days without heating. This dataset is called the *Step case*.

The second dataset is a test based on a ROLBS (Randomly Ordered Logarithmically distributed Binary Sequence) scenario, widely used in the literature (Madsen et al. 2015), generating heating steps of 115 W of random duration and uncorrelated from outdoor climatic conditions. This dataset is divided into two parts: 'identification' (13 days) and 'validation' (3 days). This means that the second part only aims at validating the final model. This dataset is called the *Rolbs case*. The identification part of the *Step case* and the *Rolbs case* have roughly the same duration. Electrical equipment in the test cell consumed 50 W non-stop.

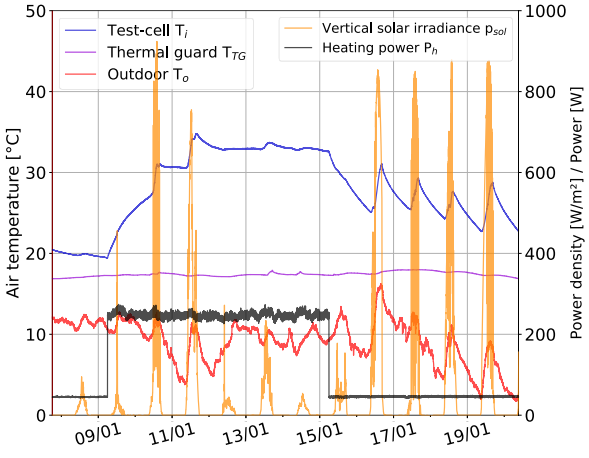

Figure 3: Measured data during the Step case

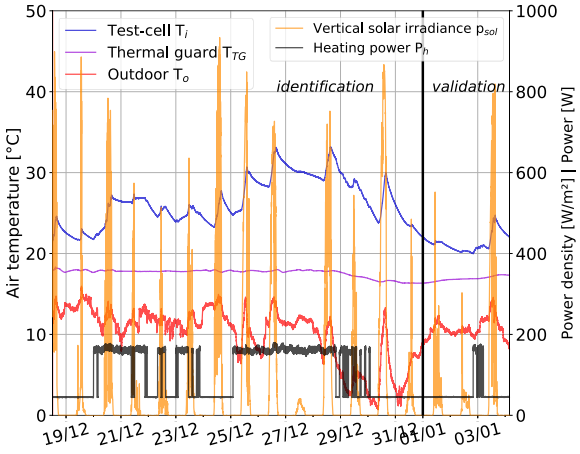

Figure 4: Measured data during the Rolbs case

Modelling

The behaviour of the cell is influenced by the thermal guard and the external environment so the model takes these two boundary conditions into account. The parameters to be identified are the thermal resistances and capacities of the *facade* and test cell, including thermal bridges, and the effective window area.

The State-Space Models

The models are a set of Resistance-Capacitance models. These dynamic thermal models are built with the CTSM-R toolkit (Kristensen and Madsen 2003). The toolkit also provides the ability to estimate model parameters by the maximisation of the the likelihood function L. The function L is the product of the conditional probabilities of measuring the temperature at time t given the temperature measured at time t-1 and the parameters to be identified. The identification is performed on the state variable T_i which represents the air temperature of the test cell. When L is maximum, the measured T_i is as close as possible to the simulated T_i. The maximum of the function is found with the quasi-Newton algorithm.

The models considered in this paper are presented in Figure 5, Figure 6, Figure 9 and in the Appendix. The simplest model is the model T_i in Figure 5 and the most complex models are the model $T_iT_fT_cR_wA_w$ in Figure 6 and the model $T_iT_fT_cA_eA_w$ in Figure 17.

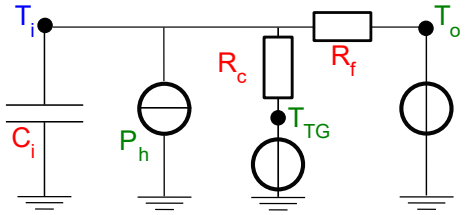

Figure 5: Model T_i

The simplest model represents the interior of the test cell using a capacity C_i and a potential T_i. This node is connected to a current generator representing the heating power P_h and to two other potentials T_{TG} and T_o. Two resistances R_c and R_f are located between the potential T_i and the potentials T_{TG} and T_o and represent the resistance between the environments.

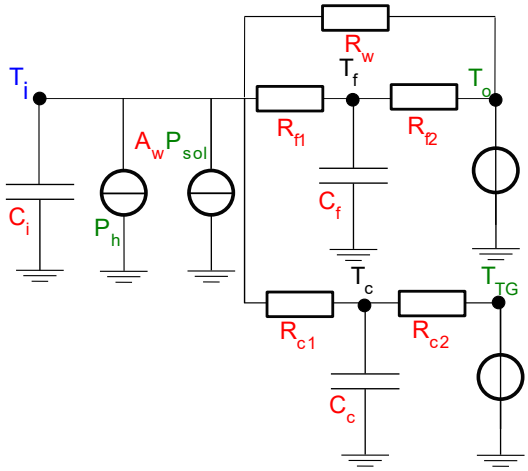

Figure 6: Model $T_iT_fT_cR_wA_w$

$T_iT_fT_cR_wA_w$ models the exchanges between environments using one capacitance and two resistances. This model also includes a current generator named A_wP_{sol} connected to the potential T_i and representing the amount of solar radiation transmitted into the cell. Also, a parallel resistance is kept between the inside and outside, R_w, in order to model the exchanges by conduction, convection and long wave radiation through the window. $T_iT_fT_cA_eA_w$

integrates a parameter A_e instead which is the effective area in which the solar radiation enters the opaque wall.

Interpretability of parameters

A_w is the effective collecting area. C_i, C_c and C_f refer respectively to the capacity of the indoor furniture, the capacity of the walls of the test cell and the capacity of the *facade*.

The total resistance of the *facade* R_f is calculated as a resistance which is equivalent to four resistances in parallel: the resistance of the opaque wall, the resistance of the wooden structure around it (in green in Figure 2 (c)), the resistance of the window and the resistance of the thermal bridge due to the window. The resistance R_f equals R_f or the sum of R_{f1} and R_{f2}. It is valid for the model T_i and for all models in the Appendix. For the model $T_iT_fT_cR_wA_w$, the resistance R_{f1}+R_{f2} does not include the window resistance (R_w) and it is named $R_{f/w}$.

The resistance of the walls of the test cell R_c (or R_{c1}+R_{c2}) is calculated as a resistance which is equivalent to four resistances in parallel: the resistance of the wall of the test cell, the resistance of the *thermal bridge due to the beams*, the resistance of the *other thermal bridges*.

Model Selection Procedure

According to (Hastie, Tibshirani, and Friedman 2009), the most appropriate model is the model that best describes the phenomenon observed experimentally while avoiding overlearning. The method described in (Bacher and Madsen 2011) was applied to find the most appropriate model among those detailed in Appendix. The method aims at studying simplified models of growing complexity. The parameters of each model are estimated using the CTSM-R toolkit in *the Step case* and *the Rolbs case* by maximizing the likelihood function. The chosen model is the latest model improving significantly the likelihood function. In addition, the residuals obtained must be independent and identically distributed (Cryer and Chan 2008).

Influence of Air Infiltration on Component Resistance

Air infiltration in the test cell is not explicitly modelled in the Resistance-Capacitance models but it has an impact on the resistances of the walls of the test cell (R_c) or on the resistance of the *facade* (R_f) depending on the air flow direction and the flow rate. In order to evaluate more precisely the influence of airtightness on the thermal balance of the test cell, the infiltration was modelled in the Contam 3.2 software© (Dols and Polidoro 2015) as illustrated in Figure 7. The test cell has two openings: a crack in the door which corresponds to a seal tightness defect and a leakage area in the *facade* determined by an air permeability test of the test cell (n_{50} = 0.74 /h).

Two situations arise depending on the location of these openings (top or bottom). In red, in Figure 7, air comes from outside through the *facade* and passes through the cell walls to reach the thermal guard. In this case, the resistance of the *facade* R_f takes infiltration into account.

In blue, in Figure 7, air comes from the thermal guard and goes to the outside through the *facade*. Then, the resistance of the walls of the test cell R_c is influenced. The resistance of the air infiltration is calculated as the inverse of the product of the airflow rate, the density and the specific heat of air.

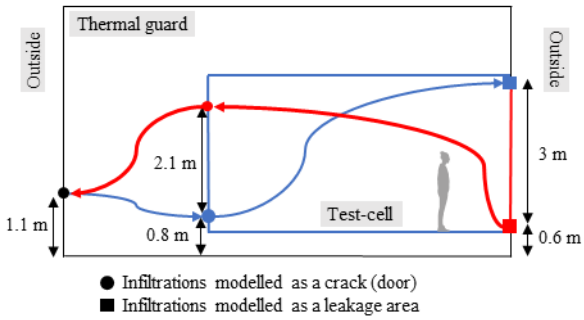

Figure 7: Position of the infiltration openings in the test cell – sectional view

The average flow rates reached in *the Rolbs case* and *the Step case* are 2.6 m^3/h (blue) and 1.3 m^3/h (red). The flow rate is almost zero if both openings are at the bottom or at the top.

Calculation of Theoretical Values

The models presented in Figure 5, Figure 6 and the appendix are based on different parameters: resistances (R_f, R_c, R_w), capacities (C_i, C_f, C_c) and an area (A_w). Table 1 gives the theoretical values of the parameters, with a lower and an upper bound when they can be calculated. An explanation of these calculations is given below.

Table 1: Summary of theoretical parameter values

Parameter	Lower limit	Upper limit	Unit
A_w	0.62	0.70	m²
R_f	0.18	0.20	K/W
$R_{f/w}$	0.50		
R_w	0.28	0.32	
R_c	0.15	0.17	
C_f	0.01	0.29	kWh/K
C_c	0.04	0.58	
C_i	0.16	0.21	

The effective window area of the *facade* (A_w)

This parameter is calculated according to the method explained in (ISO 13790 2008). It is the product of the window area (2 m²), the transparent area fraction (70%), the total solar energy transmittance of the transparent part and the shading reduction factor for external obstacles. The total solar energy transmittance of the transparent part is calculated as the product of the solar energy transmittance for radiation perpendicular to the glazing from (EN 410 2011) and a correction factor (0.9). It equals 0.58. The shading reduction factor for external obstacles is estimated from Type 34 of TRNSys software© (Solar Energy Laboratory 2009). This reduction factor is between 0.76 and 0.86 depending on the amount of direct solar radiation (calculated for the considered period). Hence, the parameter A_w is supposed to be between 0.62 and 0.70 m².

The resistance of the window (R_w)

The resistance of the window was calculated using the WINDOW 7 software© (Mitchell et al. 2019). The properties of the panes are known (U_w = 1.1 W/m²/K). A classic PVC frame was chosen in the software.

Considering a window surface of 2 m², the resistance of the window R_w is 0.32 K/W in winter conditions when there is no infiltration and 0.28 K/W when infiltration is maximum.

The resistance of the *facade* (R_f)

R_f equals 0.20 K/W if there is no infiltration. When the airflow rate is maximum, R_f equals 0.18 K/W. $R_{f/w}$ equals 0.50 K/W (infiltration is already taken into account in R_w).

The resistance of the walls of the test cell (R_c)

The *thermal bridge due to the beams* has been identified to a 1R1C model thanks to a sensor placed in the middle of the crossing and a 3D finite element model. The *other thermal bridges* have been estimated by the calibration of a coupled energy/airflow model with TRNSys 17 and Contam 3.2 softwares (Solar Energy Laboratory 2009; Khalifa et al. 2015). The resistance of the walls of the test cell R_c equals 0.17 K/W when there is no infiltration and 0.15 K/W when infiltration is maximum.

The capacity of the *facade* and the walls of the test cell (C_f and C_c)

The lower limit of capacities is determined by calculating the effective thermal capacity according to (ISO 13786 2017) considering a heating period of one hour; this period is the lowest observed on the two heating scenarios. The upper limit is the total thermal capacity calculated by considering the specific thermal capacities of each material contained in the components. The capacity C_c is between 0.04 and 0.58 kWh/K. The capacity C_f is between 0.01 and 0.24 kWh/K.

The capacity of the test cell (C_i)

An inventory of the items in the cell has been carried out. There are the composite beams, steel parts, the heating device, the fan, water in the cooling system, copper in the sensors and air. An estimation of their capacity was possible thanks to various references: the devices information and (ISO 10456 2008). C_i is estimated between 0.16 and 0.21 kWh/K.

Parameter Variation Range for Identification

The parameters are bounded in the CTSM-R tool. The boundaries are presented in Table 2.

Table 2: Range of parameters for identification

Type	Lower limit	Upper limit	Unit
Surface	10^{-3}	3	m²
Resistance	10^{-4}	0.8	K/W
Capacity	10^{-2}	0.8	kWh/K

The capacity of the test cell C_i was assessed in detail. Therefore, this parameter is allowed to vary between its lower and its upper limit. It was checked that the parameters do not hit the limits at each identification.

Methodology of Identification by Parts

The flowchart of the methodology is shown in Figure 8. C_i is bounded in each case as mentioned before. First, a lower limit and an upper limit of A_w are estimated using both datasets and for two consecutive sunny days. These values are then used to estimate the other parameters. Next, R_f and R_c are assessed using the *Step case* and its devoted model. Afterwards, the *Rolbs case* (identification part) is used with its suitable model. R_w and $R_{f/w}$ are evaluated thanks to the estimated values of A_w and R_c. The same method is applied to estimate C_f and C_c taking into account the estimated values of A_w, R_c, R_w and $R_{f/w}$. Finally, A_w is estimated given the parameters quoted above. Finally, the model is validated by comparison with experimental data considering all the estimated parameters using the *Rolbs case* (validation part).

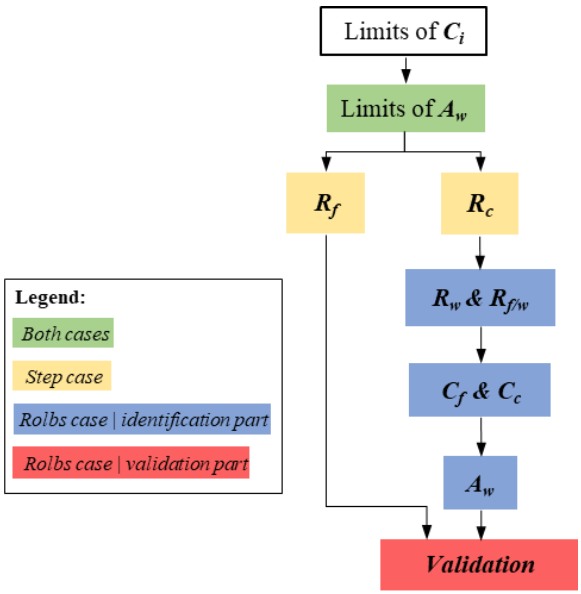

Figure 8: Flowchart of the method

Results and Discussion

The aim of the study is to estimate the above-mentioned parameters. First, the model selection procedure is applied. Then, the parameters are estimated in several steps.

Model Selection

The method selection procedure of (Bacher and Madsen 2011) is applied to the models detailed in Appendix. The best model is the latest model improving significantly the likelihood function. The result is given in Table 3 for the *Step case*. In that case, the most suitable model is the model $T_iT_fT_cA_w$ (Figure 9).

Table 3: Model selection for the Step case

Iteration	Model / L		
1	T_i		
	43997		
2	T_iT_c	T_iT_f	T_iA_w
	43997	45804	46541
3	$T_iT_fA_w$	$T_iT_cA_w$	
	48452	48459	
4	**$T_iT_fT_cA_w$**		
	48592		
5	$T_iT_fT_cA_eA_w$	$T_iT_fT_cR_wA_w$	
	48592	48593	

This means that the performances of the *facade* are identified by one capacity and two resistances. It is not possible to estimate the resistance of the window separately.

The same model selection procedure has been applied to *the Rolbs case*. In this case, the most appropriate model is the model $T_iT_fT_cR_wA_w$ (Figure 6). This indicates that it seems possible to estimate the performance of the window. This may be due to the fact that the data of this case are richer in terms of frequency and the experiment is a bit longer.

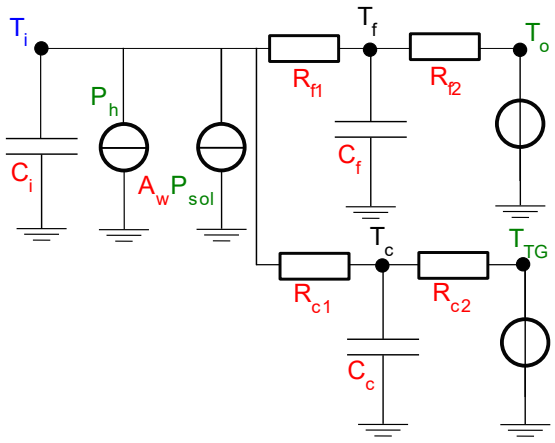

Figure 9: Model $T_i\,T_f\,T_c\,A_w$

Estimation of A_w

The parameter A_w is assumed to be constant in the models whereas it has been shown that it can vary as a function of direct solar radiation. On a cloudy day, the direct solar radiation is low and therefore the shading reduction factor for external obstacles is bigger than on a sunny day, as is A_w. Moreover, the parameter A_w cannot be estimated accurately during a day without direct solar radiation because it depends only on this boundary condition. A_w is estimated during two consecutive sunny days for the *Rolbs case* and the *Step case*. The results are shown in Table 4. The parameter is estimated between 0.84 and 1.00 m². The mean value is 0.91 m². The estimated value of A_w is higher than the theoretical values (Table 2). A final assessment of A_w is made just before the validation as shown in Figure 8. A_w equals 0.93 ± 0.03 m².

Table 4: Result of the estimation of A_w in m²

Case	*Date*	*Estimation*
Step	*16-17/01*	*0.94 ± 0.06*
Step	*18-19/01*	*0.91 ± 0.06*
Rolbs	*24-25/12*	*0.89 ± 0.05*
Rolbs	*30-31/12*	*0.89 ± 0.04*

The surface A_w is about 0.2 m² bigger than the theoretical value. This can be partly explained by the fact that the *Rolbs case* and the *Step case* include few days with high direct solar radiation and thus, the reduction factor should be lower than the estimated one. Moreover, the parameter A_w is supposed to vary according to the direct solar radiation.

Estimation of the Resistances

The resistances R_f and R_c have been estimated with the *model* $T_iT_fT_cA_w$ and the *Step case*: R_c = 0.14 ± 0.02 K/W and R_f = 0.16 ± 0.01 K/W. These values are close to the theoretical values.

The resistances $R_{f/w}$ and R_w have been estimated with the *model* $T_iT_fT_cR_wA_w$ and the identification part of the *Rolbs case*. The value of R_c was set to the value estimated above. The resistance of the *facade* without the window equals to $R_{f/w}$ = 0.37 ± 0.03 K/W and the resistance of the window is R_w = 0.28 ± 0.02 K/W. $R_{f/w}$ is lower than the theoretical value whereas R_w is the expected value. Also, the total resistance of the *facade* R_f is calculated considering the resistances $R_{f/w}$ and R_w in parallel. It equals 0.16 ± 0.01 K/W. It is the value previously given by the *model* $T_iT_fT_cA_w$ and the *Step case*.

The resistance of the walls of the test cell R_c is close to the lower limit of the theoretical value. The resistance of the *facade* without the window $R_{f/w}$ are lower than the theoretical values. Infiltrations may have been underestimated and the behaviour may be more complex than the one presented in the article. In addition, other thermal bridges may have been neglected.

Estimation of the Capacities

The capacities C_f and C_c have been estimated with the model $T_iT_fT_cR_wA_w$ and the identification part of the *Rolbs case*. The values of A_w, R_c, $R_{f/w}$ and R_w were set to the value estimated above. The capacity of the *facade* C_f equals to 0.28 ± 0.02 kWh/K and the resistance of the walls of the test cell 0.24 ± 0.02 kWh/K. This matches the theoretical values. C_i equals 0.19 kWh/K with a narrow uncertainty.

The capacity C_c is in the range of the theoretical values. The capacity C_f is close to the upper limit. This can be explained by a lack of knowledge of the thermal properties of the materials of the *facade*. Indeed, the specific heat capacities and densities were obtained from standards and have not been measured or provided by manufacturers for all materials.

Validation

In order to check that the model correctly reproduces the thermal behaviour of the test cell, the validation part of the *Rolbs case* was used. The values of A_w, $R_{f/w}$, R_f, R_c, C_f, C_c and C_i are the estimated values detailed above. Figure 10 shows the temperature measured in the test cell and the temperature estimated by the model and the residuals. The residuals are low so the model correctly reproduces the thermal behaviour of the cell. It has been verified that the residuals are independent and identically distributed.

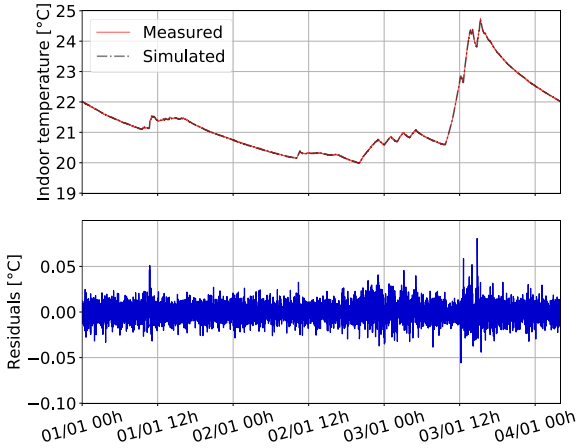

Figure 10: Temperature measured the test cell and estimated by the model and the residuals

Conclusions

A highly insulated *facade* with double glazing was characterized. Two experimental datasets were recorded: one containing a single heating step and the other describing a dynamic heating scenario. Then, an existing simplified model selection was used on each dataset. A new procedure for identifying the parameters of the most complex model has been proposed. It made it possible to take advantage of the information contained in the two datasets. The final model was validated by residual analysis.

The results shown in Figure 11 are in accordance with the estimated theoretical values except for the effective window area of the *facade* (A_w) which seems to be overestimated. Further investigation is required on this item. An experimental dataset measured during a clear sunny day could solve this problem.

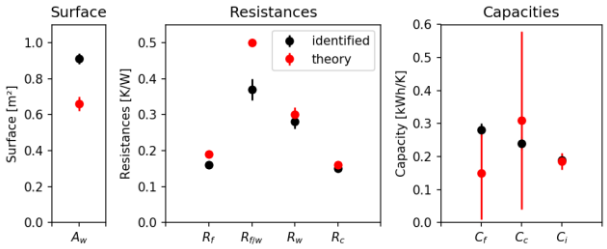

Figure 11: Comparison of theoretical and estimated values

The thermal resistance of the *facade* without the window $R_{f/w}$ and the resistance of the whole *facade* R_f are underestimated. This might be explained by the fact that a few thermal bridges may have been missed.

Acknowledgement

The activities have been carried out in the framework of the Research Project "CITEE – Innovative components for building envelopes", financed by the European Union and the French region Nouvelle-Aquitaine with the industrial partners TIPEE Platform and EDF. The authors would also like to thank Michel Burlot, David Gaillard and Laurent Servant for their contributions to the experimental work. The authors are grateful to Dynastee network and to DTU Compute for the development of the CTSM-R tool.

Appendix: RC-models

In blue, the state variable used for identification.
In black, other state variables.
In green, the boundary conditions.
In red, the parameters to be estimated.

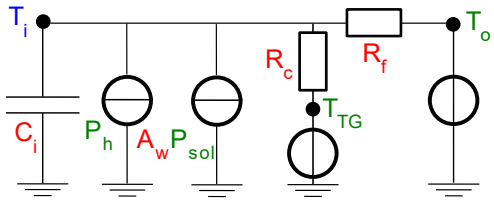

Figure 12: Model $T_i A_w$

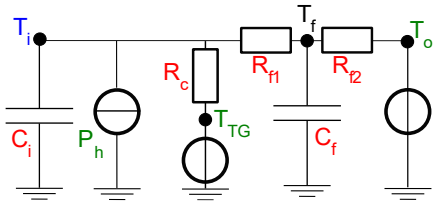

Figure 13: Model $T_i T_f$

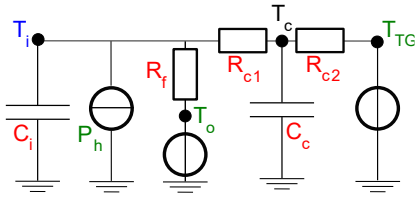

Figure 14: Model $T_i T_c$

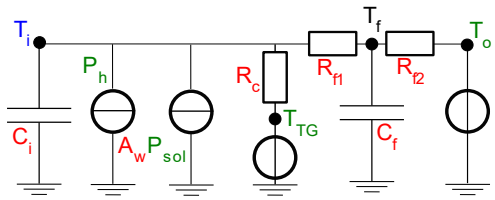

Figure 15: Model $T_i T_f A_w$

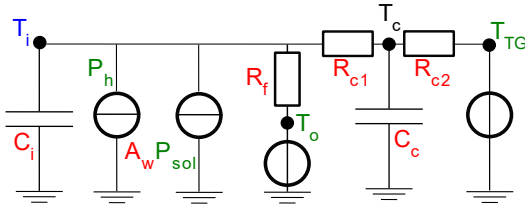

Figure 16: Model $T_i T_c A_w$

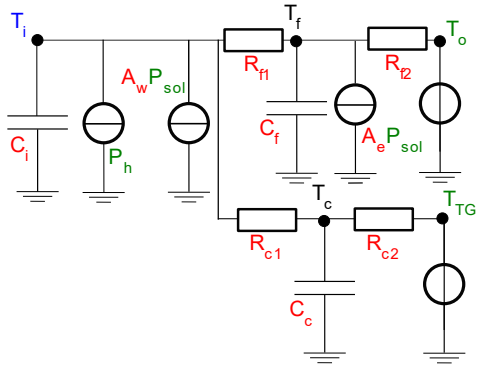

Figure 17: Model $T_i T_f T_c A_e A_w$

References

Agathokleous, Rafaela A., and Soteris A. Kalogirou. 2016. 'Double Skin Facades (DSF) and Building Integrated Photovoltaics (BIPV): A Review of Configurations and Heat Transfer Characteristics'. Renewable Energy 89 (April): 743–56. https://doi.org/10.1016/j.renene.2015.12.043.

Attia, Shady, Senem Bilir, Taha Safy, Christian Struck, Roel Loonen, and Francesco Goia. 2018. 'Current Trends and Future Challenges in the Performance Assessment of Adaptive Façade Systems'. Energy and Buildings 179 (November): 165–82. https://doi.org/10.1016/j.enbuild.2018.09.017.

Bacher, Peder, and Henrik Madsen. 2011. 'Identifying Suitable Models for the Heat Dynamics of Buildings'.

Energy and Buildings 43 (7): 1511–22. https://doi.org/10.1016/j.enbuild.2011.02.005.

Cattarin, G., F. Causone, A. Kindinis, and L. Pagliano. 2016. 'Outdoor Test Cells for Building Envelope Experimental Characterisation – A Literature Review'. Renewable and Sustainable Energy Reviews 54 (February): 606–25. https://doi.org/10.1016/j.rser.2015.10.012.

Cryer, Jonathan D., and Kung-Sik Chan. 2008. Time Series Analysis: With Applications in R. Springer Science & Business Media.

Dols, W Stuart, and Brian J Polidoro. 2015. 'CONTAM User Guide and Program Documentation Version 3.2'. National Institute of Standards and Technology. https://doi.org/10.6028/NIST.TN.1887.

EN 410. 2011. 'Glass in Building. Determination of Luminous and Solar Characteristics of Glazing'. 2011.

Favoino, Fabio, Roel Loonen, Maxime Doya, and Francesco Goia. 2018. 'Building Performance Simulation and Characterisation of Adaptive Facades – Adaptive Facade Network', 191.

Ficco, Giorgio, Fabio Iannetta, Elvira Ianniello, Francesca Romana d'Ambrosio Alfano, and Marco Dell'Isola. 2015. 'U-Value in Situ Measurement for Energy Diagnosis of Existing Buildings'. Energy and Buildings 104 (October): 108–21. https://doi.org/10.1016/j.enbuild.2015.06.071.

Freitas, Sara, and Miguel Centeno Brito. 2019. 'Solar Façades for Future Cities'. Renewable Energy Focus 31 (December): 73–79. https://doi.org/10.1016/j.ref.2019.09.002.

Gaspar, Katia, Miquel Casals, and Marta Gangolells. 2018. 'In Situ Measurement of Façades with a Low U-Value: Avoiding Deviations'. Energy and Buildings 170 (July): 61–73. https://doi.org/10.1016/j.enbuild.2018.04.012.

Gori, Virginia, Valentina Marincioni, Phillip Biddulph, and Clifford A. Elwell. 2017. 'Inferring the Thermal Resistance and Effective Thermal Mass Distribution of a Wall from in Situ Measurements to Characterise Heat Transfer at Both the Interior and Exterior Surfaces'. Energy and Buildings 135 (January): 398–409. https://doi.org/10.1016/j.enbuild.2016.10.043.

Hastie, Trevor, Robert Tibshirani, and Jerome Friedman. 2009. Elements of Statistical Learning: Data Mining, Inference, and Prediction. 2nd Edition. Springer. https://web.stanford.edu/~hastie/ElemStatLearn/.

ISO 10456. 2008. Building Materials and Products -- Hygrothermal Properties -- Tabulated Design Values and Procedures for Determining Declared and Design Thermal Values.

ISO 13786. 2017. 'Thermal Performance of Building Components — Dynamic Thermal Characteristics — Calculation Methods'. 2017.

ISO 13790. 2008. 'Energy performance of buildings — Calculation of energy use for space heating and cooling'. ISO. 2008.

Jiménez, M. J., B. Porcar, and M. R. Heras. 2008. 'Estimation of Building Component UA and GA from Outdoor Tests in Warm and Moderate Weather Conditions'. Solar Energy 82 (7): 573–87. https://doi.org/10.1016/j.solener.2008.02.013.

Juricic, Sarah, Peder Bacher, Jeanne Goffart, Simon Rouchier, Aurélie Foucquier, and Gilles Fraisse. 2019. 'Identifiability of the Heat Transfer Coefficient in Buildings with Unheated Spaces'. Proceedings of Building Simulation 2019, September 2019.

Juricic, Sarah, Simon Rouchier, Aurélie Foucquier, and Gilles Fraisse. 2018. 'Evaluation of the Physical Interpretability of Calibrated Building Model Parameters'. International Building Physics Conference, September.

Khalifa, Ines, Leila Gharbi Ernez, Essia Znouda, and Chiheb Bouden. 2015. 'Coupling TRNSYS 17 and CONTAM: Simulation of a Naturally Ventilated Double-Skin Façade'. Advances in Building Energy Research 9 (2): 293–304. https://doi.org/10.1080/17512549.2015.1050694.

Kristensen, Niels Rode, and Henrik Madsen. 2003. 'Continuous Time Stochastic Modelling - Mathematics Guide'. Technical University of Denmark, 10 December 2003.

Madsen, Henrik, Peder Bacher, Geert Bauwens, An-Heleen Deconinck, Glenn Reynders, Staf Roels, and Eline Himpe. 2015. 'Thermal Performance Characterization Using Time Series Data'. IEA EBC Annex 58 Guidelines, January, 84.

Mitchell, Robin, Christian Kohler, Dragan Curcija, Ling Zhy, Simon Vidanovic, Stephen Czarnecki, and Darius Arasteh. 2019. 'WINDOW 7 User Manual'. n Lawrence Berkeley National Laboratory.

Naveros, I., P. Bacher, D. P. Ruiz, M. J. Jiménez, and H. Madsen. 2014. 'Setting up and Validating a Complex Model for a Simple Homogeneous Wall'. Energy and Buildings 70 (February): 303–17. https://doi.org/10.1016/j.enbuild.2013.11.076.

Pflug, Thibault, Nikolaus Nestle, Tilmann E. Kuhn, Monica Siroux, and Christoph Maurer. 2018. 'Modeling of Facade Elements with Switchable U-Value'. Energy and Buildings 164 (April): 1–13. https://doi.org/10.1016/j.enbuild.2017.12.044.

Raillon, L., and C. Ghiaus. 2018. 'An Efficient Bayesian Experimental Calibration of Dynamic Thermal Models'. Energy 152 (June): 818–33. https://doi.org/10.1016/j.energy.2018.03.168.

Roels, Staf, Peder Bacher, Geert Bauwens, Sergio Castaño, Maria José Jiménez, and Henrik Madsen. 2017. 'On Site Characterisation of the Overall Heat Loss Coefficient: Comparison of Different Assessment Methods by a Blind Validation Exercise on a Round Robin Test Box'. Energy and Buildings 153 (October): 179–89. https://doi.org/10.1016/j.enbuild.2017.08.006.

Solar Energy Laboratory. 2009. 'TRNSYS 17 Volume 4 Mathematical Reference'.

Yang, Yingying. 2017. Innovative Non-Destructive Methodology for Energy Diagnosis of Building Envelope. PhD Thesis. Bordeaux, France.